Progress In Electromagnetics Research C, Vol. 121, 207–220, 2022

Self-Dual Integral Equation for Scattering Analysis from Bodies of Revolution with Multiple Impedance Boundary Conditions

Maryam Niknejad[1], Mojtaba Maddah-Ali[2], Ahmad Bakhtafrouz[1, *], and Mohsen Maddahali[1]

Abstract—In this paper, electromagnetic scattering from multi-impedance body of revolutions (BORs) is formulated using self-dual integral equations (SDIEs) and is solved numerically by the method of moments using BOR basis functions. Using the axial symmetry advantage of BORs, a 3D problem is converted to a 2D one, and a significant reduction in unknowns is obtained. This in turn leads to an increase in the speed of scattering problem solving. Numerical results show that monostatic and bistatic RCS calculation with the proposed method is about 85 and 18 times faster than the commercial software, respectively.

1. INTRODUCTION

Radar Cross Section (RCS) is one of the most important parameters in detecting an object by radar. Therefore, the calculation of this quantity plays an important role in the scattering problems and enables engineers to have a proper assessment of the behavior of the structure against electromagnetic fields before construction, which helps them in optimal design. Scattering problems are often described by integral equations. These equations are obtained by applying boundary conditions to the tangential fields. Usually, Method of Moments (MOM) is used to convert integral equations into a linear system of equations that can be solved numerically using the computer [1]. By applying the boundary conditions for tangential electric and magnetic fields on the surface of a perfect electric conductor (PEC), the electric-field integral equation (EFIE) and magnetic-field integral equation (MFIE) are obtained, respectively, and by their linear combination, combined-field integral equation (CFIE) is obtained. However, PEC is an ideal model for lossless, impenetrable scatterers, structures with infinite conductivity and materials with zero surface impedance. But there are cases that are better described with non-zero impedance or limited conductivity, so another model is needed for these situations. A suitable model is impedance boundary condition (IBC) [2]. In addition to modeling the losses and finite conductivity of the metals, IBC is used to model coated conducting bodies, rough surfaces [3], corrugated surfaces [4], and other configurations [5–7]. In the IBC model, electric and magnetic fields on the surface of an object are related to each other by surface impedance [8]. This model simplifies the analysis of scattering problems because surface electric and magnetic currents are related by surface impedance, and there is no need to calculate the fields within the structure. After obtaining the equivalent surface impedance and the surface integral equation for the scattering problem, a common approach is to eliminate the equivalent electric or magnetic current using IBC [9]. But similar to the PEC scattering problems, IBC-EFIE and IBC-MFIE have problems with the resonant frequency when being applied to closed surfaces, and therefore IBC-CFIE is usually preferred [10–12]. But when the method of moment is used to discretize and convert IBC-CFIE to matrix equations, this formulation faces some

Received 19 May 2022, Accepted 29 June 2022, Scheduled 22 July 2022

* Corresponding author: Ahmad Bakhtafrouz (bakhtafrouz@iut.ac.ir).

[1] Department of Electrical and Computer Engineering, Isfahan University of Technology, Isfahan 84156-83111, Iran. [2] Department of Electroceramics and Electrical Engineering, Malek Ashtar University of Technology, 83157-13115, Iran.

challenges. When the surface impedance approaches the free space impedance, an ill-conditioned matrix is obtained [13]. Also, if the RWG functions are used to expand the magnetic current, a contour integral of artificial line charge is created [14]. The ill-conditioned matrix and contour integral cause instability and slow convergence of the matrix system, in which case the answer of the numerical method will be unreliable. Many studies have been done to solve these problems [15–19]. In [20], a novel surface integral equation formulation is proposed by including both the electric and magnetic currents as individual unknown quantities, and the impedance boundary condition is used implicitly in the surface integral equations rather than imposed explicitly. It is also demonstrated that the proposed formulation in [20] is well posed in terms of different surface impedances and different mesh densities.

Among various types of geometries, axial symmetry geometry has been used in many applications, which is called body of revolution. Bodies of revolution (BORs) are generated by rotating a generating arc around the axis of symmetry. These structures are of particular importance due to their application in measurement calibration, modeling of real targets, and use as benchmark targets to validate new methods. Until now extensive efforts have been made to analyze the scattering from BORs [21–24]. In order to calculate the radar cross section of BOR structures, the surface integral equation is first written in terms of equivalent electric and magnetic currents. Then by using rotationally symmetrical property, the integral equation is discretized by a set of basis functions that are local on the boundary curve along the longitudinal direction and a Fourier series in the azimuthal direction. Because different Fourier modes are independent, the system of equations is solved separately for each mode. Therefore, both the memory requirement and calculation time can be reduced greatly compared to traditional methods (method of moment (MoM) based on sub-domain basis functions, such as Rao-Wilton-Glisson (RWG) basis functions).

In this paper, the radar cross section of multi-impedance BORs is calculated using the SDIE formulation by the current expansion with BOR basis functions, which causes significant reduction of unknowns. Therefore, the memory requirement and CPU time for obtaining the RCS of BORs are improved greatly than [20]. Several examples are given to verify the validity and efficiency of the proposed method. The rest of the paper is organized as follows. The formulation of SDIE for scattering by arbitrarily IBC is proposed in Section 2. In Section 3, the method of moment and BOR basis functions are used to convert integral equations to a linear system of equations. The formulation for scattering from bodies of revolution with multi-impedance boundary conditions is obtained in this section. In Section 4, several numerical examples are presented to illustrate the accuracy and efficiency of the proposed method. At last, a brief conclusion is given in Section 5.

2. FORMULATION

In this section, the formulation of SDIE for scattering by arbitrarily IBC objects is first proposed. The proposed formulation is then used to calculate the scattering from BOR with impedance boundary conditions.

2.1. Self-Dual Integral Equations

Consider electromagnetic scattering from an impedance object with boundary S, which is immersed in a free space with intrinsic impedance of η and illuminated by an incident plane wave ($\mathbf{E}^{\text{inc}}$, $\mathbf{H}^{\text{inc}}$). The electric and magnetic field integral equations (EFIE, MFIE) on the surface can be formulated in terms of the equivalent surface electric current $\tilde{\mathbf{J}} = \eta\mathbf{J}$ and magnetic current $\mathbf{M}$ in matrix form as

$$\begin{bmatrix} \Gamma & -\frac{I}{2} + \Psi \\ \frac{I}{2} - \Psi & \Gamma \end{bmatrix} \begin{bmatrix} \tilde{\mathbf{J}} \\ \mathbf{M} \end{bmatrix} = \begin{bmatrix} \hat{\mathbf{n}} \times \mathbf{E}^{\text{inc}} \\ \hat{\mathbf{n}} \times \tilde{\mathbf{H}}^{\text{inc}} \end{bmatrix} \tag{1}$$

where $\tilde{\mathbf{H}}^{\text{inc}} = \eta\mathbf{H}^{\text{inc}}$, I denotes the identity operator, and Ψ and Γ are the integral operators defined as

$$\Gamma(X) = ik\hat{\mathbf{n}} \times \int_S \left[I + \frac{1}{k^2}\nabla\nabla\cdot \right] G(\mathbf{r}, \mathbf{r}')\mathbf{X}(\mathbf{r}')d\mathbf{r}' \tag{2}$$

$$\Psi(\mathbf{X}) = \hat{\mathbf{n}} \times P.V. \int_S \nabla G(\mathbf{r}, \mathbf{r}') \times \mathbf{X}(\mathbf{r}') d\mathbf{r}' \tag{3}$$

where $G(\mathbf{r}, \mathbf{r}') = e^{-ik|\mathbf{r}-\mathbf{r}'|}/4\pi|\mathbf{r}-\mathbf{r}'|$ is the free space Green's function with the wave number k; $\mathbf{X}$ represents either $\tilde{\mathbf{J}}$ or $\mathbf{M}$; and *P.V.* stands for the Cauchy principal value integration.

The EFIE and MFIE formulas in (1) are dependent in essence. So another independent equation is needed to determine $\tilde{\mathbf{J}}$ and $\mathbf{M}$ uniquely. For structures that can be modeled with the surface impedance, which are the interest in this article, according to the impedance boundary condition [2], the relation between $\mathbf{J}$ and $\mathbf{M}$ is given as

$$\mathbf{M} = -Z_s \hat{\mathbf{n}} \times \mathbf{J} \tag{4}$$

Or equivalently

$$\mathbf{J} = \frac{1}{Z_s} \hat{\mathbf{n}} \times \mathbf{M} \tag{5}$$

which can be written in terms of $\tilde{\mathbf{J}}$ and $\mathbf{M}$ as

$$\begin{bmatrix} z_s \hat{\mathbf{n}} \times I & I \\ -I & \dfrac{1}{z_s} \hat{\mathbf{n}} \times I \end{bmatrix} \begin{bmatrix} \tilde{\mathbf{J}} \\ \mathbf{M} \end{bmatrix} = \begin{bmatrix} 0 \\ 0 \end{bmatrix} \tag{6}$$

where z_s is the normalized surface impedance ($z_s = Z_s/\eta$). Therefore, (1) equipped with (6) gives rise to a complete set of equations for IBC problems

$$\begin{bmatrix} z_s \hat{\mathbf{n}} \times I + \Gamma & I/2 + \Psi \\ -I/2 - \Psi & \dfrac{1}{z_s} \hat{\mathbf{n}} \times I + \Gamma \end{bmatrix} \begin{bmatrix} \tilde{\mathbf{J}} \\ \mathbf{M} \end{bmatrix} = \begin{bmatrix} \hat{\mathbf{n}} \times \mathbf{E}^{\text{inc}} \\ \hat{\mathbf{n}} \times \tilde{\mathbf{H}}^{\text{inc}} \end{bmatrix} \tag{7}$$

However, since the magnitudes of the diagonal blocks in the above operator matrix are proportional to z_s, the condition number of the matrix is highly dependent on the z_s changes. To overcome this problem, the first line in (6) is divided into $\sqrt{z_s}$, and the second line is multiplied by $\sqrt{z_s}$ to obtain

$$\begin{bmatrix} \sqrt{z_s} \hat{\mathbf{n}} \times I & I \\ -\sqrt{z_s} I & \hat{\mathbf{n}} \times I \end{bmatrix} \begin{bmatrix} \tilde{\mathbf{J}} \\ \tilde{\mathbf{M}} \end{bmatrix} = \begin{bmatrix} 0 \\ 0 \end{bmatrix} \tag{8}$$

where $\tilde{\mathbf{M}} = \mathbf{M}/\sqrt{z_s}$, and Equation (1) can then be rewritten as

$$\begin{bmatrix} \Gamma & -\dfrac{I}{2} + \Psi \\ \dfrac{I}{2} - \Psi & \Gamma \end{bmatrix} \begin{bmatrix} \tilde{\mathbf{J}} \\ \sqrt{z_s} \tilde{\mathbf{M}} \end{bmatrix} = \begin{bmatrix} \hat{\mathbf{n}} \times \mathbf{E}^{\text{inc}} \\ \hat{\mathbf{n}} \times \tilde{\mathbf{H}}^{\text{inc}} \end{bmatrix} \tag{9}$$

In the case where the normalized surface impedance is a constant, Equation (9) becomes

$$\begin{bmatrix} \Gamma & -\dfrac{\sqrt{z_s}}{2} + \sqrt{z_s}\Psi \\ \dfrac{1}{2} - \Psi & \sqrt{z_s}\,\Gamma \end{bmatrix} \begin{bmatrix} \tilde{\mathbf{J}} \\ \tilde{\mathbf{M}} \end{bmatrix} = \begin{bmatrix} \hat{\mathbf{n}} \times \mathbf{E}^{\text{inc}} \\ \hat{\mathbf{n}} \times \tilde{\mathbf{H}}^{\text{inc}} \end{bmatrix} \tag{10}$$

The summation of (8) and (10) then yields

$$\begin{bmatrix} \sqrt{z_s} \hat{\mathbf{n}} \times I + \Gamma & -\dfrac{\sqrt{z_s}}{2} + 1 + \sqrt{z_s}\Psi \\ \dfrac{1}{2} - \sqrt{z_s} - \Psi & \hat{\mathbf{n}} \times I + \sqrt{z_s}\Gamma \end{bmatrix} \begin{bmatrix} \tilde{\mathbf{J}} \\ \tilde{\mathbf{M}} \end{bmatrix} = \begin{bmatrix} \hat{\mathbf{n}} \times \mathbf{E}^{\mathbf{inc}} \\ \hat{\mathbf{n}} \times \tilde{\mathbf{H}}^{\mathbf{inc}} \end{bmatrix} \tag{11}$$

Since the magnitudes of all the blocks of the operator matrix are proportional to $\sqrt{z_s}$, the condition of the matrix equation is much less sensitive to z_s.

Equation (11) is known as the self-dual integral equation (SDIE) for uniform surface impedance cases. In the case where the normalized impedance is a function of position, Equation (11) can only be written as

$$\begin{bmatrix} \sqrt{z_s} \hat{\mathbf{n}} \times I + \Gamma & -\dfrac{\sqrt{z_s}}{2} + 1 + \Psi(\sqrt{z_s}) \\ \dfrac{1}{2} - \sqrt{z_s} - \Psi & \hat{\mathbf{n}} \times I + \Gamma(\sqrt{z_s}) \end{bmatrix} \begin{bmatrix} \tilde{\mathbf{J}} \\ \tilde{\mathbf{M}} \end{bmatrix} = \begin{bmatrix} \hat{\mathbf{n}} \times \mathbf{E}^{\mathbf{inc}} \\ \hat{\mathbf{n}} \times \tilde{\mathbf{H}}^{\mathbf{inc}} \end{bmatrix} \tag{12}$$

Since z_s is a function of position in this case, and the calculations will be complicated, the summation of (8) and (9) in terms of $\tilde{\mathbf{J}}$ and $\mathbf{M}$ yields

$$\begin{bmatrix} \sqrt{z_s}\hat{\mathbf{n}}\times I+\Gamma & -\frac{1}{2}+\frac{1}{\sqrt{z_s}}+\Psi \\ \frac{1}{2}-\sqrt{z_s}-\Psi & \frac{1}{\sqrt{z_s}}\hat{\mathbf{n}}\times I+\Gamma \end{bmatrix} \begin{bmatrix} \tilde{\mathbf{J}} \\ \mathbf{M} \end{bmatrix} = \begin{bmatrix} \hat{\mathbf{n}}\times\mathbf{E}^{\mathbf{inc}} \\ \hat{\mathbf{n}}\times\tilde{\mathbf{H}}^{\mathbf{inc}} \end{bmatrix} \tag{13}$$

Equation (13) is known as the self-dual integral equation (SDIE) for nonuniform surface impedance cases.

3. BOR-MOM

To obtain scattering from bodies of revolution with impedance boundary conditions, we use method of moments (MOM) to convert (11) or (13) into a linear system of equations that can be solved numerically using a computer. In this process, we use the axial symmetry feature of BORs to simplify calculations.

A BOR object is generated by rotating a generating arc around an axis of symmetry. Therefore, we define such an object in the cylindrical coordinate system as shown in Fig. 1.

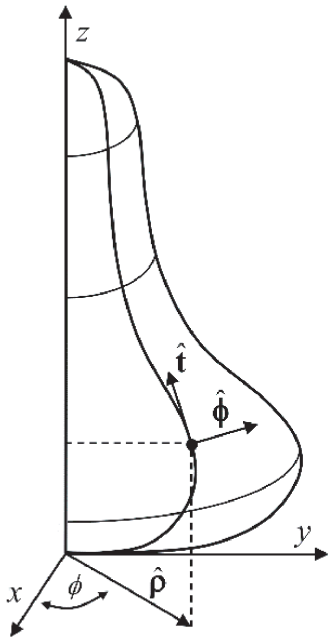

Figure 1. BOR surface outline.

We next define the longitudinal vector $\hat{\mathbf{t}}(\mathbf{r})$, which, along with the cylindrical vector $\hat{\phi}(\mathbf{r})$, is everywhere tangent to the surface and forms the orthogonal set with the surface normal $\hat{\mathbf{n}}(\mathbf{r})$:

$$\hat{\mathbf{n}}(\mathbf{r}) = \hat{\phi}(\mathbf{r}) \times \hat{\mathbf{t}}(\mathbf{r}) \tag{14}$$

As $\hat{\mathbf{t}}(\mathbf{r})$ and $\hat{\phi}(\mathbf{r})$ are everywhere normal to each other, we will represent the surface currents using $\hat{\mathbf{t}}(\mathbf{r})$ and $\hat{\phi}(\mathbf{r})$ oriented basis functions. Because of the rotational symmetry, these functions are local in the longitudinal dimension and a Fourier series in the azimuthal dimension

$$\mathbf{J}(\mathbf{r}) = \sum_{\alpha=-\infty}^{\infty}\sum_{n=1}^{N}\left[a_{\alpha n}^{t}\mathbf{f}_{\alpha n}^{t}(\mathbf{r}) + a_{\alpha n}^{\phi}\mathbf{f}_{\alpha n}^{\phi}(\mathbf{r})\right] \tag{15}$$

$$\mathbf{M}(\mathbf{r}) = \sum_{\alpha=-\infty}^{\infty}\sum_{n=1}^{N}\left[K_{\alpha n}^{t}\mathbf{f}_{\alpha n}^{t}(\mathbf{r}) + K_{\alpha n}^{\phi}\mathbf{f}_{\alpha n}^{\phi}(\mathbf{r})\right] \tag{16}$$

where $I^t_{\alpha n}$, $K^t_{\alpha n}$ are the longitudinal expansion coefficients of basis function n for Fourier mode α, and $I^\phi_{\alpha n}$ and $K^\phi_{\alpha n}$ are the azimuthal expansion coefficients for mode α and basis function n.

The expansion functions $\mathbf{f}^{t,\phi}_{\alpha n}(\mathbf{r})$ are

$$\begin{aligned}\mathbf{f}^t_{\alpha n}(\mathbf{r}) &= f_n(t)\, e^{j\alpha\phi}\hat{\mathbf{t}}(\mathbf{r})\\ \mathbf{f}^\phi_{\alpha n}(\mathbf{r}) &= f_n(t)\, e^{j\alpha\phi}\hat{\phi}(\mathbf{r})\end{aligned} \tag{17}$$

where $f_n(t) = T_n(t)/\rho(t)$, and $T_n(t)$ is the triangular function. In the expansion of surface currents for BORs, the various Fourier modes are perpendicular to each other. This property is very useful, so the system of equations can be solved separately for each mode, and the final solution is obtained by adding the answers for each mode.

Method of moment is used to convert (11) and (13) into a matrix system. Surface currents from (15), (16) are substituted, and then SDIEs will be tested using testing functions $\mathbf{f}^{t,\phi}_{\beta m}(\mathbf{r})$.

$$\begin{aligned}\mathbf{f}^t_{\beta m}(\mathbf{r}) &= f_m(t)\, e^{-j\beta\phi}\hat{\mathbf{t}}(\mathbf{r})\\ \mathbf{f}^\phi_{\beta m}(\mathbf{r}) &= f_m(t)\, e^{-j\beta\phi}\hat{\phi}(\mathbf{r})\end{aligned} \tag{18}$$

In (11), (13), there are in total four operators namely, Γ, Ψ, I, and $\hat{\mathbf{n}}\times I$ which are discretized as follows

$$\begin{aligned}\Gamma^{pq}_{mn} &= jk\iint_{\mathbf{f}^{t,\phi}_{\beta m}}\iint_{\mathbf{f}^{t,\phi}_{\alpha n}} \mathbf{f}^{t,\phi}_{\beta m}(\mathbf{r})\cdot\left[\hat{\mathbf{n}}(\mathbf{r})\times\mathbf{f}^{t,\phi}_{\alpha n}(\mathbf{r}')\right]\frac{e^{-jkr}}{4\pi r}d\mathbf{r}'d\mathbf{r}\\ &\quad -\frac{j}{k}\iint_{\mathbf{f}^{t,\phi}_{\beta m}}\iint_{\mathbf{f}^{t,\phi}_{\alpha n}}\left[\nabla\cdot\left(\mathbf{f}^{t,\phi}_{\beta m}(\mathbf{r})\times\hat{\mathbf{n}}(\mathbf{r})\right)\right]\left[\nabla'\cdot\mathbf{f}^{t,\phi}_{\alpha n}(\mathbf{r}')\right]\frac{e^{-jkr}}{4\pi r}d\mathbf{r}'d\mathbf{r} \qquad (19)\\ \Psi^{pq}_{mn} &= \frac{1}{4}\iint_{\mathbf{f}^{t,\phi}_{\beta m}}\iint_{\mathbf{f}^{t,\phi}_{\alpha n}}\mathbf{f}^{t,\phi}_{\beta m}(\mathbf{r})\cdot\hat{\mathbf{n}}(\mathbf{r})\\ &\quad\times\left[-(\mathbf{r}-\mathbf{r}')\times\mathbf{f}^{t,\phi}_{\alpha n}(\mathbf{r}')\right]\cdot[1+jkr]\frac{e^{-jkr}}{r^3}d\mathbf{r}'d\mathbf{r} \qquad (20)\\ I^{pq}_{mn} &= \int_{\mathbf{f}^{t,\phi}_{\beta m}}\mathbf{f}^{t,\phi}_{\beta m}(\mathbf{r})\cdot\mathbf{f}^{t,\phi}_{\alpha n}(\mathbf{r})d\mathbf{r} \qquad (21)\\ (\hat{\mathbf{n}}\times I)^{pq}_{mn} &= \int_{\mathbf{f}^{t,\phi}_{\beta m}}\mathbf{f}^{t,\phi}_{\beta m}(\mathbf{r})\cdot\hat{\mathbf{n}}\times\mathbf{f}^{t,\phi}_{\alpha n}(\mathbf{r})d\mathbf{r} \qquad (22)\end{aligned}$$

where p and q may be either t or ϕ.

Applying the testing functions $\mathbf{f}^{t,\phi}_{\beta m}(\mathbf{r})$ to the right-hand side of (11) or (13) yields a column vector of the form

$$\mathbf{V} = \begin{bmatrix}\mathbf{V}^t_E\\ \mathbf{V}^\phi_E\\ \mathbf{V}^t_M\\ \mathbf{V}^\phi_M\end{bmatrix} \tag{23}$$

where

$$\begin{aligned}\mathbf{V}^{t,\phi}_E(m) &= \int_{t_m}\int_0^{2\pi}\mathbf{f}^{t,\phi}_{\alpha m}(\mathbf{r})\cdot\left(\hat{\mathbf{n}}\times\mathbf{E}^{\text{inc}}(\mathbf{r})\right)\rho d\phi dt \qquad (24)\\ \mathbf{V}^{t,\phi}_M(m) &= \int_{t_m}\int_0^{2\pi}\mathbf{f}^{t,\phi}_{\alpha m}(\mathbf{r})\cdot\left(\hat{\mathbf{n}}\times\tilde{\mathbf{H}}^{\text{inc}}(\mathbf{r})\right)\rho d\phi dt \qquad (25)\end{aligned}$$

After solving the matrix equations and obtaining the unknown coefficients of surface currents, the scattered far electric field will be as follows

$$\mathbf{E}(\mathbf{r}) = -j\omega\left(\left[\mathbf{A}_\theta(\mathbf{r})+\eta\mathbf{F}_\phi(\mathbf{r})\right]\hat{\theta}+\left[\mathbf{A}_\phi(\mathbf{r})-\eta\mathbf{F}_\theta(\mathbf{r})\right]\hat{\phi}\right) \tag{26}$$

where in the far field, the vector potentials are written as follows

$$\mathbf{A}(\mathbf{r}) = \mu \frac{e^{-jkr}}{4\pi r} \int_V \mathbf{J}(\mathbf{r}') e^{jk\mathbf{r}'\cdot\hat{\mathbf{r}}} d\mathbf{r}' \tag{27}$$

$$\mathbf{F}(\mathbf{r}) = \varepsilon \frac{e^{-jkr}}{4\pi r} \int_V \mathbf{M}(\mathbf{r}') e^{jk\mathbf{r}'\cdot\hat{\mathbf{r}}} d\mathbf{r}' \tag{28}$$

Finally, the radar cross section for the object is calculated from:

$$\sigma_{3D} = 4\pi r^2 \frac{|\mathbf{E}^s|^2}{|\mathbf{E}^{\text{inc}}|^2} \tag{29}$$

4. NUMERICAL RESULT

In this section, several numerical examples are presented to illustrate the accuracy and efficiency of proposed approach. Responses of the proposed method in bistatic mode, in addition to IE-based commercial software, have also been verified by time domain solver of CST that is based on the finite integration technique (FIT). All problems are solved on the same computer (Intel(R) Core(TM) i7-7500, 2.7 GHz and 8 GB RAM) in order to make a fair comparison.

4.1. Uniform Cases

In this section, in order to show the performance of the proposed formulation, the radar cross section is calculated in two modes, monostatic and bistatic. The two structures shown in Fig. 2 are studied at two frequencies of $f_1 = 0.5\,\text{GHz}$ and $f_2 = 1\,\text{GHz}$ with $\hat{\theta}$ and $\hat{\phi}$ polarization. The results are shown in Fig. 3 to Fig. 6. Other specifications of the analyzed structures are mentioned in the caption of the figures. The results are compared with the solutions from commercial software. Figures show that an excellent agreement is achieved between the solution of the proposed approach and the commercial software solution.

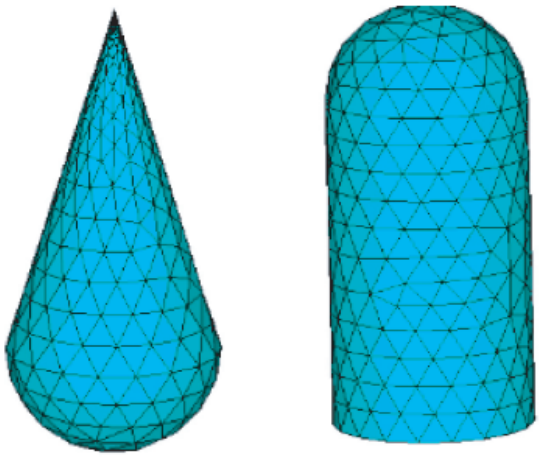

Figure 2. Mono-impedance objects.

4.2. Nonuniform Cases

To demonstrate the performance of the proposed method, scattering problems from BORs with nonuniform surface impedance, such as Fig. 7, are presented in this section. The radar cross section is calculated in two modes, monostatic and bistatic. Structures have been studied at two frequencies of $f_1 = 0.5\,\text{GHz}$ and $f_2 = 1\,\text{GHz}$ with $\hat{\theta}$ and $\hat{\phi}$ polarization. Specifications of the analyzed structures are

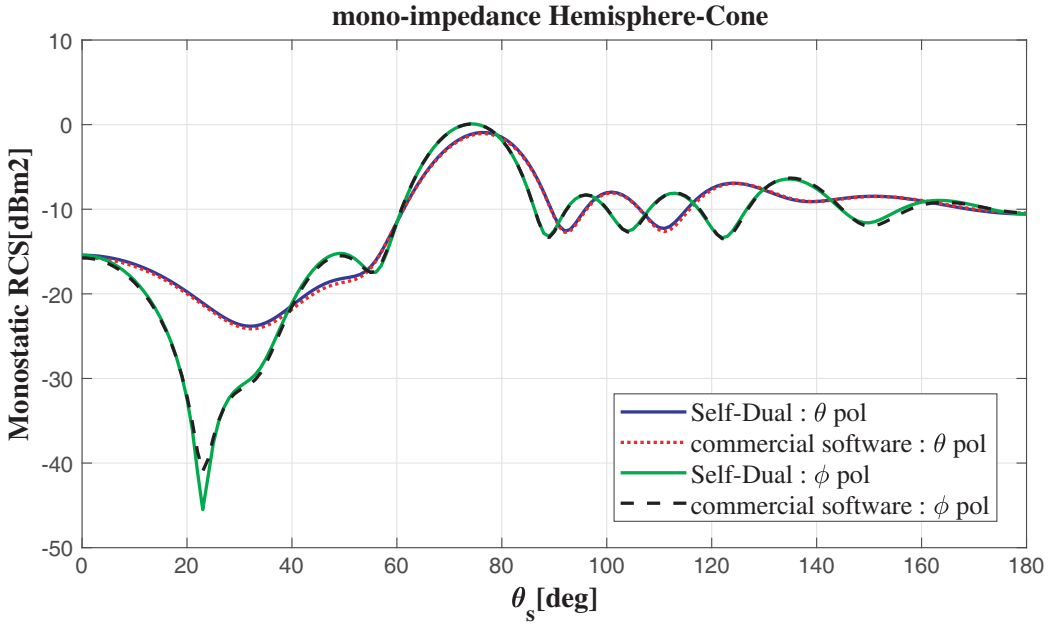

Figure 3. Monostatic RCS of mono-impedance Hemisphere-Cone at $f_1 = 0.5\,\text{GHz}$. when $R = 0.3\,\text{m} = 0.5\lambda_1$, $h = 1.3\,\text{m} = 2.16\lambda_1$ and $Z_s = 5$.

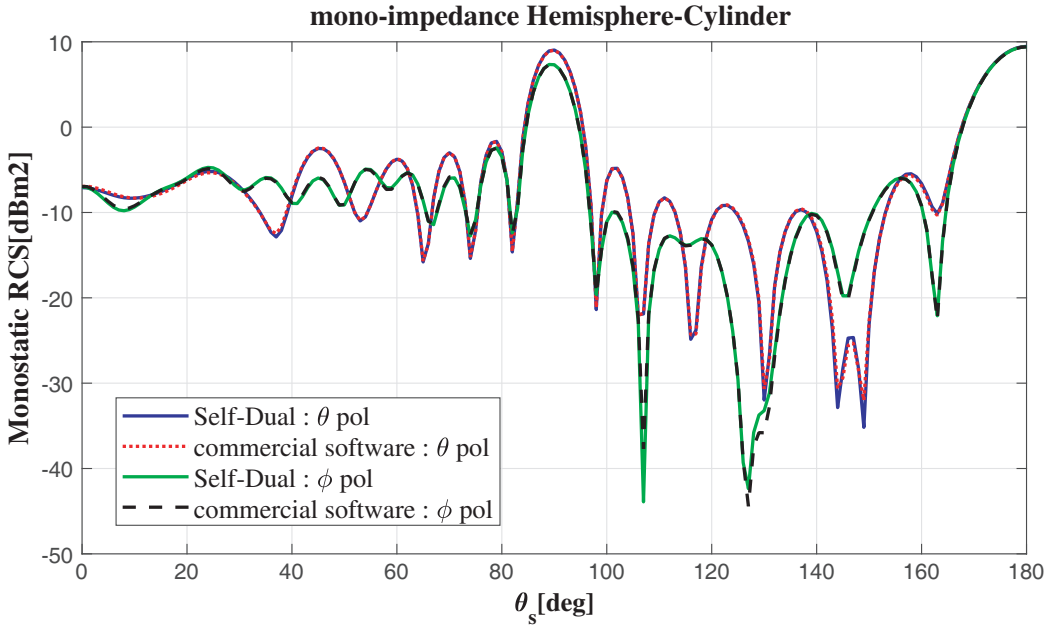

Figure 4. Monostatic RCS of mono-impedance Hemisphere-Cylinder $f_2 = 1\,\text{GHz}$. when $R = 0.3\,\text{m} = \lambda_2$, $h = 1.3\,\text{m} = 4.32\lambda_2$ and $Z_s = 0.4 - 2i$.

mentioned in the caption of the figures. The results are compared with the solutions from commercial software (Fig. 8 to Fig. 11).

As can be seen, the results of the numerical implementation of the integral equations with the expansion of currents in terms of BOR basic functions are in excellent agreement with the simulation results of commercial software.

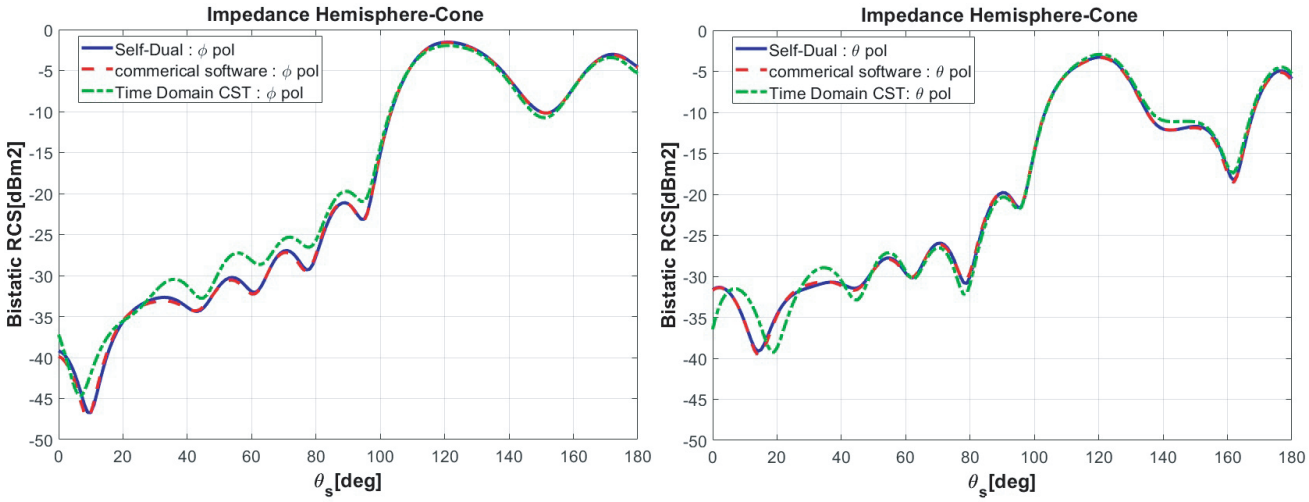

Figure 5. Bistatic RCS of mono-impedance Hemisphere-Cone at $f_2 = 1\,\text{GHz}$. when $R = 0.3\,\text{m} = \lambda_2$, $h = 1.3\,\text{m} = 4.32\lambda_2$, $\theta^i = 30$, $\phi^i = 45$, $\phi^s = 60$ and $Z_s = 0.5 + 0.5i$. (a) ϕ polarization. (b) θ polarization.

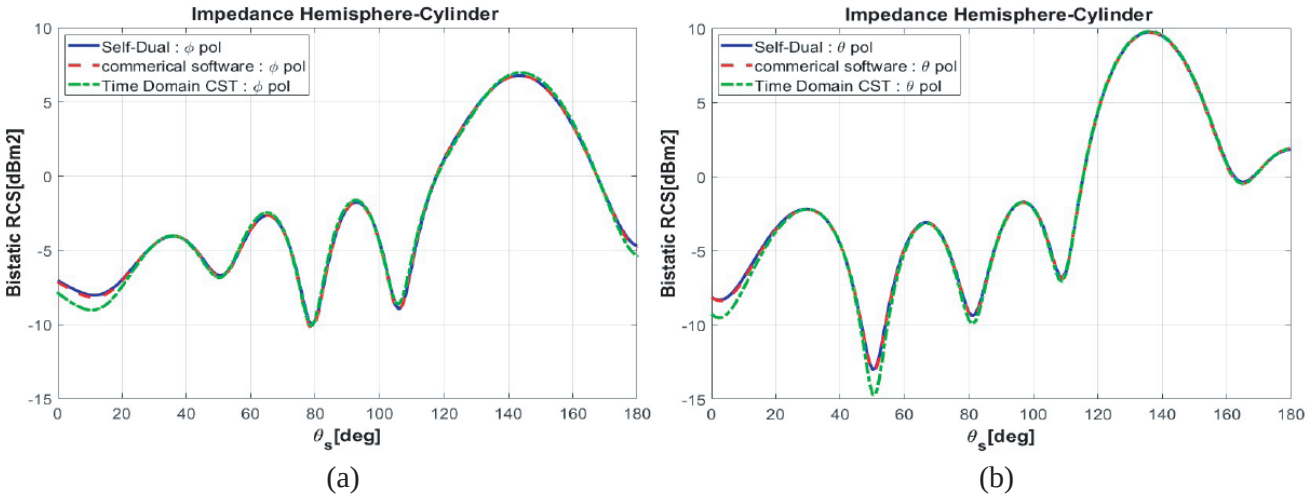

Figure 6. Bistatic RCS of mono-impedance Hemisphere-Cylinder at $f_1 = 0.5\,\text{GHz}$. when $R = 0.3\,\text{m} = 0.5\lambda_1$, $h = 1.3\,\text{m} = 2.16\lambda_1$, $\theta^i = 45$, $\phi^i = 180$, $\phi^s = 45$ and $Z_s = 0.1 + 0.2i$. (a) ϕ polarization. (b) θ polarization.

4.3. Efficiency Comparison

In order to demonstrate the efficiency of the presented method in this paper, for several problems, the computation time of RCS using the presented method and that of commercial software (CST Microwave Studio) are compared in Table 1 for mono-impedance Hemisphere-cone and Table 2 for multi-impedance Hemisphere-cylinder.

In the first example, the monostatic RCS for a Hemisphere-Cone with dimensions $R = 0.3 = \lambda_2$ and $h = 1.3 = 4.32\lambda_2$, once with a surface impedance of $Z_s = 5$ and again with a surface impedance of $Z_s = 0.4 - i$ is evaluated at the frequency of $f_2 = 1\,\text{GHz}$. The results in Table 1 show that the time required to calculate RCS using commercial software is on average 85 times that calculated using the SDIE-BOR method.

In the second example, a hemisphere-cylinder with dimensions $R = 0.3 = \lambda_2$, $h = 1.3 = 4.32\lambda_2$ and

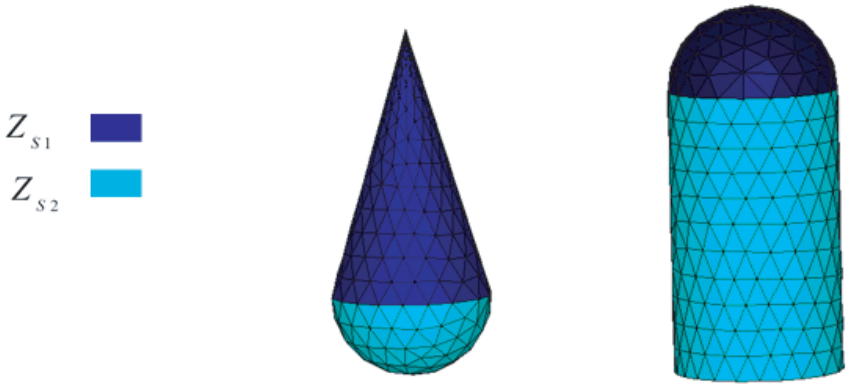

Figure 7. Multi-impedance objects.

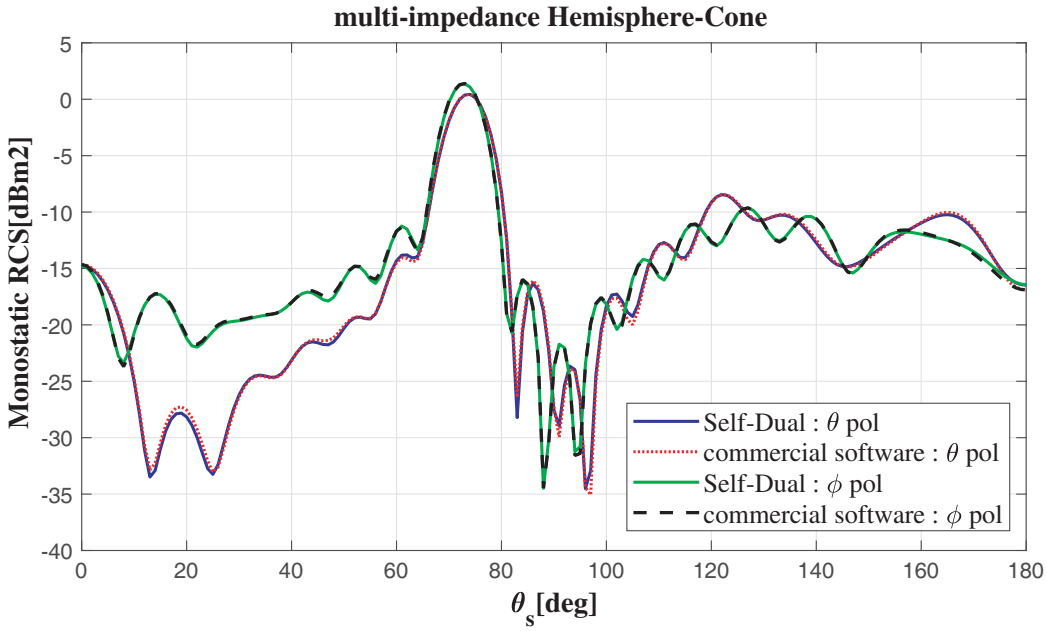

Figure 8. Monostatic RCS of multi-impedance Hemisphere-Cone at $f_2 = 1\,\text{GHz}$. when $R = 0.3\,\text{m} = \lambda_2$, $h = 1.3\,\text{m} = 4.32\lambda_2$ and $Z_{s1} = 4$, $Z_{s2} = 0.5 + 0.5i$.

Table 1. Time comparison of the SDIE-BOR method with CST Microwave Studio for mono-impedance Hemisphere-cone.

Hemisphere-Cone	$Z_s = 5$ θ pol	$Z_s = 5$ ϕ pol	$Z_s = 0.4 - i$ θ pol	$Z_s = 0.4 - i$ ϕ pol
CST	663 s	614 s	615 s	682 s
SDIE-BOR	7.36 s	7.41 s	7.86 s	7.46 s
Ratio $(t_{CST}/t_{SDIE-BOR})$	90.1	82.9	78.2	91.4

surface impedance of $Z_{s_1} = 3$, $Z_{s_2} = 0.2$ is evaluated. The bistatic RCS is computed at $f_2 = 1\,\text{GHz}$ in two cases, once with $\theta^i = 60 \quad \phi^i = 30 \quad \phi^s = 90$ and again with $\theta^i = 45 \quad \phi^i = 90 \quad \phi^s = 45$. Table 2 gives the calculation time for the proposed method and commercial software. The time required to

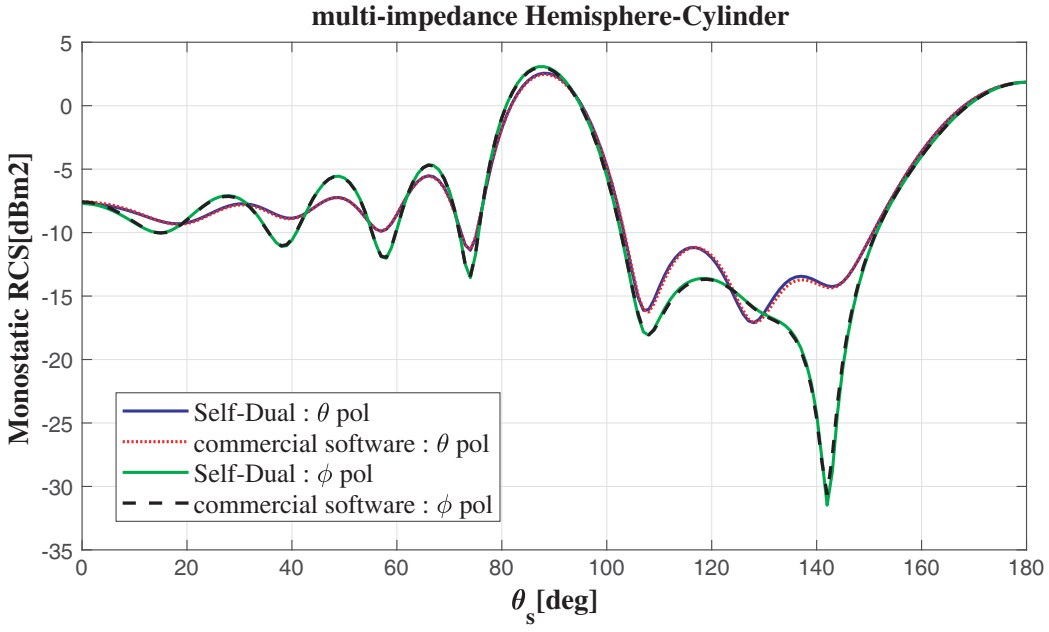

Figure 9. Monostatic RCS of multi-impedance Hemisphere-Cylinder at $f_1 = 0.5\,\text{GHz}$. when $R = 0.3\,\text{m} = 0.5\lambda_1$, $h = 1.3\,\text{m} = 2.16\lambda_1$ and $Z_{s1} = 5 + 1.5i$, $Z_{s2} = 1 + 2i$.

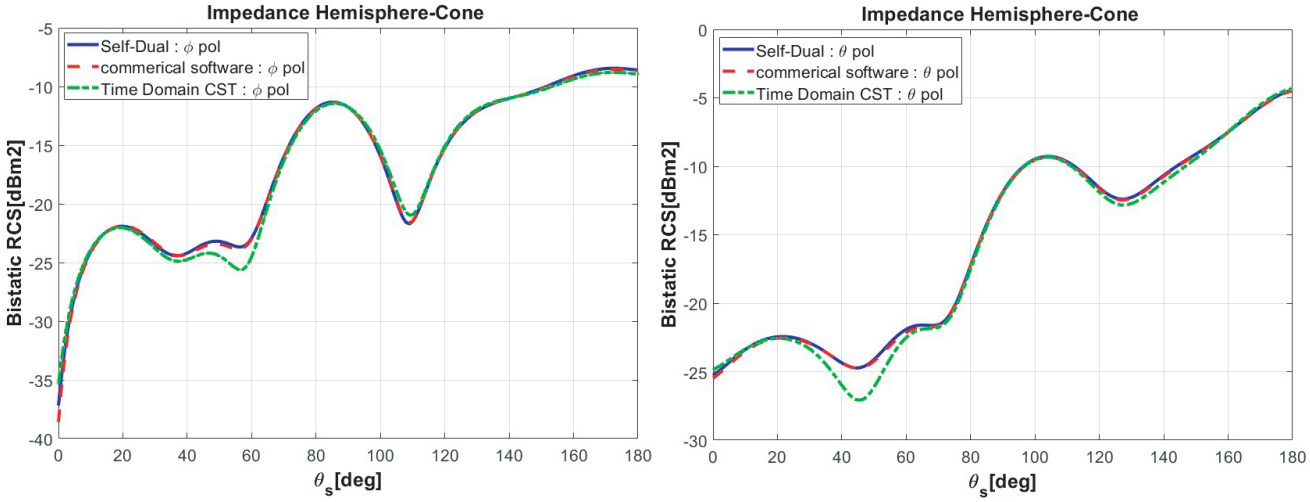

Figure 10. Bistatic RCS of multi-impedance Hemisphere-Cone at $f_1 = 0.5\,\text{GHz}$. when $R = 0.3\,\text{m} = 0.5\lambda_1$, $h = 1.3\,\text{m} = 2.16\lambda_1$, $\theta^i = 60$, $\phi^i = 30$, $\phi^s = 45$ and $Z_{s1} = 1.2$, $Z_{s2} = 2 + 3i$. (a) ϕ polarization. (b) θ polarization.

calculate RCS using commercial software is on average 18 times that calculated using the SDIE-BOR method.

The last example was performed to compare the efficiency of presented method with respect to the one of [20]. In this example, the bistatic RCS of a Hemisphere-Cone (Fig. 7) is computed for θ-polarization at $f_2 = 1\,\text{GHz}$ with $\theta^i = 45$, $\phi^i = 0$ *and* $\phi^s = 0$. It must be noticed that in this example a sector of hemisphere is selected as the bottom part of object. The cone dimensions are $R = 0.5 = 1.67\lambda_2$, $h = 1 = 3.33\lambda_2$ while the sphere radius is $R = 1.12 = 3.73\lambda_2$. The surface impedances are $Z_{s_1} = 0.25$ and $Z_{s_2} = 0.75$. Again, the RCSs from two methods are in very good agreement as shown in Fig. 12,

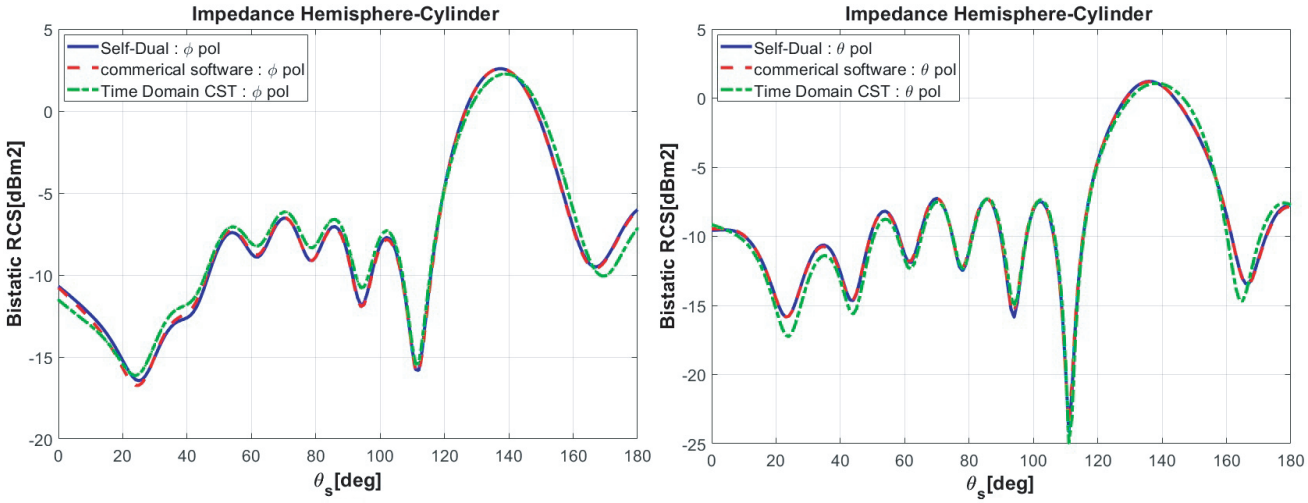

(a) (b)

Figure 11. Bistatic RCS of multi-impedance Hemisphere-Cylinder at $f_2 = 1\,\text{GHz}$. when $R = 0.3\,\text{m} = \lambda_2$, $h = 1.3\,\text{m} = 4.32\lambda_2$, $\theta^i = 45$, $\phi^i = 90$, $\phi^s = 45$ and $Z_{s1} = 3$, $Z_{s2} = 0.2$. (a) ϕ polarization. (b) θ polarization.

Table 2. Time comparison of the SDIE-BOR method with CST Microwave Studio for multi-impedance Hemisphere-cylinder.

Hemisphere-cylinder	case1 θ pol	case1 ϕ pol	case2 θ pol	case2 ϕ pol
CST	23 s	31 s	27 s	27 s
SDIE-BOR	1.55 s	1.43 s	1.42 s	1.42 s
Ratio $(t_{CST}/t_{SDIE-BOR})$	14.8	21.7	19	19

but our presented method is 180 times faster than the method of [20]. Furthermore, the required peak memory for our method is about 1000 times lower than [20]. The details of comparison are shown in Table 3.

Table 3. Time and memory comparison of the SDIE-BOR method with method of [20] for multi-impedance Hemisphere-cone (Fig. 12).

Hemisphere-cone	Time	Memory
This paper	7 s	1.62 MB
[20]	1261 s	1356 MB
Ratio ([20]/This paper)	180	1000

Finally to illustrate the well posedness of the matrix equations obtained using the proposed method, one of the examples presented in [20] is evaluated using the SDIE formulation and the BOR basis functions, and the condition number diagram is plotted in terms of mesh density (Fig. 13). The object is an IBC sphere with a radius of 1.0 m and a normalized surface impedance $z_s = 2 - 0.5i$, and the frequency of the incident plane wave is 75 MHz. As can be observed, the proposed method has a very small condition number, which increases linearly with respect to the mesh density.

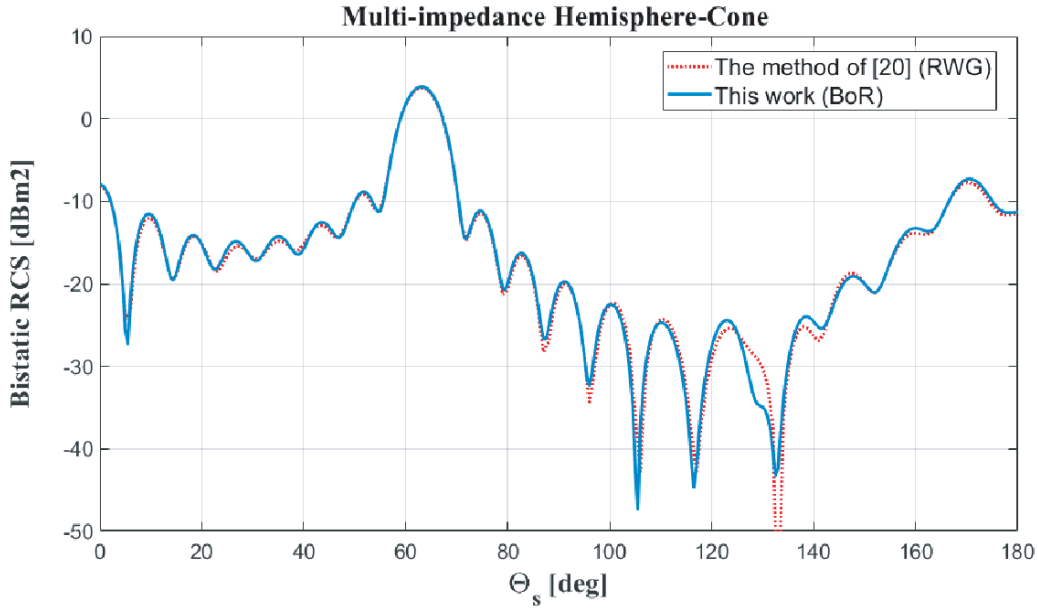

Figure 12. Bistatic RCS of multi-impedance Hemisphere-Cone at $f_2 = 1\,\text{GHz}$. when $R = 0.3\,\text{m} = \lambda_2$, $h = 1.3\,\text{m} = 4.32\lambda_2$, $\theta^i = 45$, $\phi^i = 0$, $\phi^s = 0$ and $Z_{s1} = 0.25$, $Z_{s2} = 0.75$.

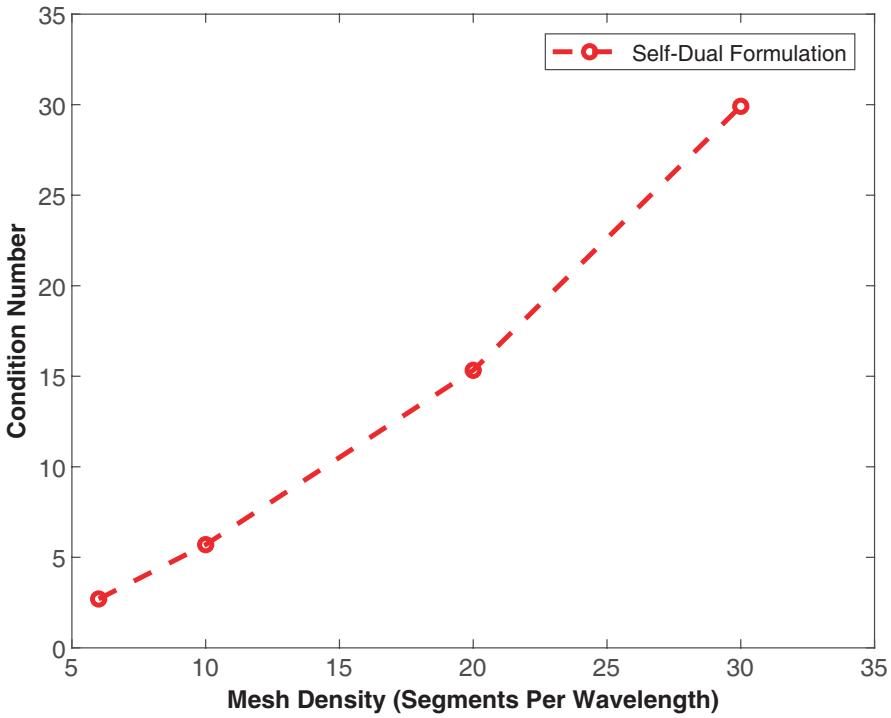

Figure 13. Condition number of the system matrix obtained from the discretization of the SDIE using BOR basis functions versus the mesh density. The object is an IBC sphere with a radius of 1.0 m and a normalized surface impedance $z_s = 2 - 0.5i$. The frequency of the incident plane wave is 75 MHz.

5. CONCLUSION

In this paper, SDIE-BOR method is proposed to analyze scattering from multi-impedance BORs. In order to avoid the problems of EFIE-IBC, MFIE-IBC, and CFIE-IBC formulations, self-dual integral equations are used to calculate the scattering of structures with impedance surfaces. In this formulation, both electric and magnetic surface currents were considered as unknown, and the impedance boundary condition was implicitly embedded in the equations. These equations were discretized using the method of moment and BOR basis functions. Using BOR basis functions, a 3D problem is converted to a 2D problem. Therefore, both the memory requirement and CPU time can be reduced greatly. The performance of the proposed method was demonstrated by some numerical examples. Excellent agreement was obtained between the results using the proposed method and commercial software. In addition, the RCS calculation time and memory were significantly reduced, which is more noticeable for large electrical structures.

REFERENCES

1. Gibson, W. C., *The Method of Moments in Electromagnetics*, CRC Press, 2014.
2. Hoppe, D. J., *Impedance Boundary Conditions in Electromagnetics*, CRC Press, 2018.
3. Senior, T., "Impedance boundary conditions for statistically rough surfaces," *Applied Scientific Research*, Section B, Vol. 8, No. 1, 437–462, 1960.
4. Iskander, K., L. Shafai, A. Frandsen, and J. Hansen, "Application of impedance boundary conditions to numerical solution of corrugated circular horns," *IEEE Transactions on Antennas and Propagation*, Vol. 30, No. 3, 366–372, 1982.
5. Senior, T., "Combined resistive and conductive sheets," *IEEE Transactions on Antennas and Propagation*, Vol. 33, No. 5, 577–579, 1985.
6. Mitzner, K., "Effective boundary conditions for reflection and transmission by an absorbing shell of arbitrary shape," *IEEE Transactions on Antennas and propagation*, Vol. 16, No. 6, 706–712, 1968.
7. Lindell, I. V. and A. H. Sihvola, "Realization of impedance boundary," *IEEE Transactions on Antennas and Propagation*, Vol. 54, No. 12, 3669–3676, 2006.
8. Yuferev, S. V. and N. Ida, *Surface Impedance Boundary Conditions: A Comprehensive Approach*, CRC Press, 2018.
9. Glisson, A. W., "Electromagnetic scattering by arbitrarily shaped surfaces with impedance boundary conditions," *Radio Science*, Vol. 27, No. 06, 935–943, 1992.
10. Sebak, A. and L. Shafai, "Scattering from arbitrarily-shaped objects with impedance boundary conditions," *IEE Proceedings H — Microwaves, Antennas and Propagation*, Vol. 136, No. 5, 371–376, IET, 1989.
11. Heath, G., "Impedance boundary condition integral equations," *1984 Antennas and Propagation Society International Symposium*, Vol. 22, 697–700, IEEE, 1984.
12. P. Ylä-Oijala, S. P. Kiminki, and S. Järvenpää, "Solving IBC-CFIE with dual basis functions," *IEEE Transactions on Antennas and Propagation*, Vol. 58, No. 12, 3997–4004, 2010.
13. Chang, A., K. Yee, and J. Prodan, "Comparison of different integral equation formulations for bodies of revolution with anisotropic surface impedance boundary conditions," *IEEE Transactions on Antennas and Propagation*, Vol. 40, No. 8, 989–991, 1992.
14. Collino, F., F. Millot, and S. Pernet, "Boundary-integral methods for iterative solution of scattering problems with variable impedance surface condition," *Progress In Electromagnetics Research*, Vol. 80, 1–28, 2008.
15. Bendali, A., M. Fares, and J. Gay, "A boundary-element solution of the Leontovitch problem," *IEEE Transactions on Antennas and Propagation*, Vol. 47, No. 10, 1597–1605, 1999.
16. Chang, A., K. Yee, and J. Prodan, "Comparison of different integral equation formulations for bodies of revolution with anisotropic surface impedance boundary conditions," *IEEE Transactions on Antennas and Propagation*, Vol. 40, No. 8, 989–991, 1992.

17. Collard, B., M. Fares, and B. Souny, "A new formulation for scattering by impedant 3D bodies," *Journal of Electromagnetic Waves and Applications*, Vol. 20, No. 10, 1291–1298, 2006.
18. Collino, F., F. Millot, and S. Pernet, "Boundary-integral methods for iterative solution of scattering problems with variable impedance surface condition," *Progress In Electromagnetics Research*, Vol. 80, 1–28, 2008.
19. Ylä-Oijala, P., S. P. Kiminki, and S. Järvenpää, "Solving IBC-CFIE with dual basis functions," *IEEE Transactions on Antennas and Propagation*, Vol. 58, No. 12, 3997–4004, 2010.
20. Yan, S. and J.-M. Jin, "Self-dual integral equations for electromagnetic scattering from ibc objects," *IEEE Transactions on Antennas and Propagation*, Vol. 61, No. 11, 5533–5546, 2013.
21. Mautz, J. R. and R. Harrington, "Radiation and scattering from bodies of revolution," *Applied Scientific Research*, Vol. 20, No. 1, 405–435, 1969.
22. Wu, T.-K. and L. L. Tsai, "Scattering from arbitrarily-shaped lossy dielectric bodies of revolution," *Radio Science*, Vol. 12, No. 5, 709–718, 1977.
23. Yuceer, M., J. R. Mautz, and E. Arvas, "Method of moments solution for the radar cross section of a chiral body of revolution," *IEEE Transactions on Antennas and Propagation*, Vol. 53, No. 3, 1163–1167, 2005.
24. Bao, J., D. Wang, and E. K. Yung, "Electromagnetic scattering from an arbitrarily shaped biisotropic body of revolution," *IEEE Transactions on Antennas and Propagation*, Vol. 58, No. 5, 1689–1698, 2010.